Post-fire Performance of Wire-arc Sprayed Zn-15Al Coatings

Ratna Divya Yasoda^a, Ying Huang^{a*}, Ravi Kiran^b, and Xiaoning Qi^c

^a Department of Civil, Construction, and Environmental Engineering., North Dakota State University, Fargo, USA Email: ratna.yasoda@ndus.edu; ying.huang@ndsu.edu

^b School of Sustainable Engineering and the Built Environment, Arizona State University, Tempe, USA
Email: ravi.kiran@asu.edu

^c Department of Coatings and Polymeric Materials, North Dakota State University, Fargo, USA Email: xiaoning.qi@ndsu.edu.

* Corresponding author

Abstract

Wire-arc sprayed Zn-15Al coatings are used to mitigate corrosion in steel infrastructure such as pipelines, offshore platforms, and bridges that are susceptible to fire due to the handling of flammable products and wildfire events, etc. Past studies indicate that steel retains its engineering properties when exposed to fire temperatures up to 600°C. Therefore, this paper aims to assess the performance of Zn-15Al protective coatings after being subjected to a fire accident. For this purpose, coated steel plates were subjected to temperatures ranging from 300°C to failure at 100°C intervals in a furnace simulating the fire accidents. Post-fire microstructural characterization, mechanical integrity tests, and electrochemical studies were performed on the coating. The coating was intact primarily when cooled from 500°C due to limited high-temperature oxidation and formation of intermetallic phases of zinc and aluminum including eutectoid $(\alpha+\eta)$, partially converted eutectic $(\beta+\eta)$ and a zinc-rich η -phase. These changes in the coating microstructure resulted in increased microhardness and consistent wear loss and an increase in the coating's electrochemical impedance compared to its as-deposited condition favoring the reusability of the coated steel members. However, at 600°C the presence of large quantities of oxidation products increased the porosity and decreased the mechanical properties of the coating. Furthermore, the separation of the zinc-rich matrix from the coating occurred and made the crosssection look like galvanized steel retaining corrosion protection ability. Micro-cracks indicating

coating failure were noticed when cooled from 700°C, and it is hence the Zn-15Al coatings should be replaced when temperatures exceed 600°C.

Keywords: Fire; Residual life of coatings; Thermally sprayed coatings; Microstructure; and High-temperature oxidation.

Introduction

Structural steels with metallic protective coatings are commonly employed to mitigate the corrosion degradation in the steel and to increase the service life of the structure, especially in offshore and marine environments [1]. Among several coating application processes, thermal spray technology is becoming more attractive owing to its high processing speed, versatility, and flexibility in obtaining the desired thickness of coatings [2]. Among these thermal spray coatings, zinc (Zn), aluminum (Al), and their alloys are the most popularly used anti-corrosive coatings for steel structures, including bridges, offshore platforms, equipment, and steel oil and gas pipelines due to their combined barrier and cathodic protection mechanisms [3]. Much research has been conducted to investigate these Zn-Al coatings' mechanical properties and corrosion performance [4-6]. Specifically, Zn-15Al (85 wt.% zinc and 15 wt.% aluminum) coatings have shown better corrosion protection compared to pure zinc and pure aluminum coatings for corrosion mitigation in chloride environments [7,8], and therefore few studies focusing on investigating the corrosion mechanism in these coatings are also available [9-12].

Although corrosion protection is enhanced in the steel infrastructure with thermally sprayed Zn-Al protective coatings, these structures are also vulnerable to fire. For instance, steel structures such as offshore platforms and oil and gas pipelines that transport flammable hydrocarbons pose fire and explosion threats [13,14]. According to the pipeline and hazardous materials safety administration (PHMSA), about 1,200 incidents of fire accidents and explosions occurred in the oil and gas pipelines industry over the past ten years [15], which resulted in an economic loss of approximately US \$ 5.4 billion and some incidents also resulted in fatalities. Moreover, bridges and other transportation facilities are also highly susceptible to fire-induced damage, caused by a multitude of events, including tanker truck accidents [16,17], wildfires [18],

and bushfires [19]. Recent studies documenting fire incidents and associated losses in transportation infrastructure [20] have shown that the average annual fire losses in bridges (in the United States) alone are estimated to be \$1.28 billion [21].

Many of the above-mentioned pipeline incidents occurred, despite the considerable efforts made to monitor and detect the leaks and spills in the oil and gas pipelines, and platforms through regular maintenance and inspection. On the other hand, accidental fire on transportation infrastructure such as bridges is not preventable. While there is a need to develop strategies for enhanced fire safety such as the identification of critical structures for fire hazards, it is also necessary to develop fire-resistant materials[22,23] and to evaluate the residual life of coated steel structural components exposed to high-temperature fires. This would help minimize the losses incurred due to repair, rehabilitation, and replacement of the coated structural steel components.

Extensive literature exists to investigate the post-fire mechanical properties of different grades of steel including mild steel, high-strength steel, and very high-strength steel [24-27]., A key takeaway from all the published work on the post-fire behavior of steels is that important mechanical properties such as yield strength, ultimate tensile strength, and ductility remain unaffected when the structural steels are subjected to elevated temperatures up to 600°C and, therefore can be reused. However, these structural steel members are often protected by either organic coatings or metallic coatings, or a combination of the two to mitigate corrosion [28-30]. Therefore, it is important to investigate the post-fire properties and behavior of these protective coatings on steels when exposed to a fire incident. Conventionally used organic coatings such as epoxy and polyurethane resins cannot withstand temperatures beyond 150°C and hence will be destroyed when exposed to a fire incident [31]. On the other hand, coatings of zinc and aluminum which are commonly employed as surface treatment for steels have melting points of 420°C and

660°C respectively and hence can withstand much higher elevated temperatures [32]. In addition, as the organic coatings have a much lower melting point of less than 150°C, the combination of the top seal with a polymer layer on the zinc and aluminum coatings would not contribute to the post-fire properties. To date, very limited information is available on the performance of these metallic coatings when exposed to high temperatures of fire. For instance, William I K McLean et al. [33] investigated the performance of hot dip galvanized steel members during bushfires. In this study, a grid of liquid propane burners was utilized to recreate a bushfire and found that the maximum air temperature recorded during the study was 675°C. The results of the study indicated that the galvanized coating was found to be intact at that temperature. However, this study was conducted on galvanized steel only and did not include the changes in the microstructure, mechanical properties, or corrosion performance.

To the best of the authors' knowledge, no literature on the post-fire performance of metal coatings specifically thermally sprayed Zn-15Al coatings is available. The objective of the present study is to investigate the post-fire behavior of wire-arc sprayed Zn-15Al coatings on structural steels. The coating's performance was assessed by investigating the changes in microstructure, mechanical properties, and electrochemical corrosion behavior after exposure to target elevated temperatures ranging from 300°C to 700°C at 100°C intervals. The details of the experimental plan, along with the important observations and results obtained, are presented in the subsequent sections of the manuscript.

Zn-15Al Coatings Application Procedure and Properties

ASTM A36 structural steel plates (50 mm x 50 mm) were used as the substrate steel. The substrate steel was grit blasted with alumina to ensure good coating adhesion. Commercially available Zn-15Al alloy wires of diameter 3.175mm were used as feedstock material in the wire-

arc spray gun (Thermion, USA) to deposit Zn-15Al alloy coating on the grit-blasted steel plates [9]. The grit blasted plates underwent a three-pass coating application, with the spray distance set to 180mm, and current and voltage parameters of 150 Amps and 32 Volts respectively. Air at an inlet pressure of 0.62 MPa, was utilized as the pressurized gas during the coating deposition process. As the top seal would not contribute to the post-fire properties, no sealing was applied on the metallic coatings. The thickness of the as-deposited coating was measured using the scanning electron microscope (SEM) images obtained from the coatings' cross-section. The produced coating had a thickness of $400 \pm 50 \mu m$. In addition, energy dispersive spectroscopy (EDS) and Xray diffraction (XRD) analyses were carried out on the as-deposited coating to determine the chemical composition and phases present in the coating, respectively. The surface SEM image, EDS spectra, and XRD pattern obtained from the Zn-15Al coating in as-deposited conditions are presented in Fig. 1. From EDS analysis, Zn-15Al as-deposited coating consisted of 79.78 wt.% zinc and 17.08 wt.% of aluminum and 3.15 wt.% oxygen (see Fig. 1(d)). In addition, the porosity analysis showed that the coating had 6.47 % porosity in the as-deposited condition (see Fig. 10). The low oxygen content and low porosity suggest the superior quality of the produced coating. Moreover, from the XRD analysis, the phases present in the coating were identified as pure zinc and pure aluminum with no additional intermetallic phases of zinc and aluminum (see Fig. 1(b)). This indicated that the wire arc sprayed Zn-15Al formed on the grit blasted substrate steel primarily through mechanical bonding, which refers to the physical bonding between the coating and the substrate due to the deformation of the coating material during the spray process that creates a mechanical interlock between the coating and the substrate [34].

High-temperature Testing of Wire-arc Sprayed Zn-15Al Coatings

The Zn-15Al coated steel specimens were heated from room temperature to a pre-selected temperature level ranging from 300°C to until failure at an interval of 100°C. The electric furnace (Thermal systems Inc, CA, USA) shown in Fig. 2 was used in this study to achieve desired target elevated temperatures. The initial high temperature of 300°C was chosen, keeping in view the Zn-15Al aluminum binary phase diagram (see Fig. 3), according to which no major phase changes are expected for Zn-15Al alloy when exposed temperatures are below 280°C. In addition, the electric furnace used in this work has a tolerance limit of ± 20 °C, and therefore temperatures less than 300°C are not considered in the present study. The simulation of fire temperatures using an electric furnace with a rate of heating inside the furnace between 10 to 15°C/min, was followed in several past studies [35,36] that targeted characterizing the post-fire properties of engineering metals and hence adopted in the present work for consistency. After reaching the target elevated temperature, the Zn-15Al coated steel specimens were left in the furnace for one hour of soaking time to ensure uniform temperature distribution across the coating and substrate. After the soaking time, the specimens were removed from the furnace and left outside to cool down to room temperature. These specimens were then utilized to evaluate the changes in the coating microstructure, porosity, phase composition, microhardness, wear resistance, and electrochemical corrosion behavior.

Morphology and Microstructural Characterization

After exposure to elevated temperatures, the coating's microstructural features such as metallurgical phase composition, phase morphology or solute in the matrix, and grain size can change. These microstructural changes alter the coating's effectiveness compared to the original coatings that were not exposed to high temperatures. Additionally, the insights obtained from the microstructural characterization would help assess the integrity of the coating. Moreover, the phase

changes dictate the mechanical performance of coatings as well [25]. Therefore, various material characterization tests were conducted in this study. Firstly, SEM imaging was performed on the coating to observe the changes in microstructural features, metal volatilization, if any, and porosity. In the present study, SEM operated at 15kV (JOEL JSM-6490 LV) was utilized to examine the surface and cross sections of Zn-15Al coated steel plates at room temperature and after being cooled from different elevated temperatures. In addition, the changes in chemical composition and oxidation of the coating were analyzed using EDS available in the SEM. Moreover, porosity changes in the coating were estimated from Zn-15Al coating microstructure through SEM images taken on the cross sections of the coating at room temperature and after being cooled from different target elevated temperatures using ImageJ software. A minimum of 6 SEM images from a specific temperature-exposed specimen were put through the analysis to get a reasonable estimate of porosity. Furthermore, X-ray diffraction analysis (XRD) was carried out on the as-deposited Zn-15Al coatings and after being cooled from elevated temperatures, since the metallurgical phases on the coating's surface play an important role in the coating's post-fire behavior when exposed to an aggressive corrosive environment. A Bruker D8 discover diffractometer was utilized to perform XRD analysis. The XRD peaks were identified/ characterized as per the inorganic crystal structure database (ICSD). To prepare specimens suitable for the characterization tests, metallographic sample preparation of the coatings was done. Asdeposited and post-fire Zn-15Al coated plates were sectioned with the help of a precision cutter and mounted in phenolic resin. These mounted surfaces and cross-sections were then ground using grit sizes up to 1200 and polished to achieve a finish that is suitable for conducting the characterization tests [37].

Mechanical Properties Evaluation

Microhardness testing on the Zn-15Al coating provides the material's mechanical response/ resistance to deformation under applied load. In addition, the relative changes in the microhardness represent the changes in the engineering properties of the Zn-15Al coating including elasticity and strength, after being cooled from the different target elevated temperatures. In the present work, the Vickers test was used to measure the microhardness of the coating, where a diamond-shaped indenter with a 136° included angle was used. An applied load of 0.1 kgf (100 gram-force) and an application time/dwell time of 15 sec were used. The Vickers hardness number (HV) also known as the diamond pyramid hardness number (DPH) was then calculated from the size of the impression that was produced under a pyramid-shaped diamond indenter as follows:

$$HV = 1.854 \times (F/D^2) \tag{Eq 1}$$

where, F is the applied load measured in kgf and D^2 is the projected area of the indentation measured in mm².

The wear/abrasion resistance of the coating is another important parameter to assess the coating's durability in addition to the microhardness. Superior wear resistance represents the coating's resilience to cutting and fragmentation by hard abrasives. The most popular wear tests include pin-on-disk and Taber abrasion [38,39]. To conduct the pin-on-disk wear test, the average surface roughness of the test specimens should be less than 0.8 μm according to ASTM standard G99-17, which otherwise makes the scar/wear track measurements difficult [40]. In the present work, since the Zn-15Al coating thickness is approximately 400μm, it is very difficult to achieve an average surface roughness of less than 0.8 μm on the entire coating surface without exposing

the substrate steel. On the other hand, the Taber abrasion test is primarily designed to evaluate the wear performance of organic coatings. Although harsher abrasive wheels (such as CS -17) [41] can be used for testing the wear performance of harder surfaces like metals and ceramics, this test also requires a very smooth surface finish on both sides of the specimen. In addition, Taber abrasion can only be performed on square-shaped specimens of size 100 mm x 100 mm or 100 mm diameter disks with a 6.50 mm central hole. Therefore, considering the practical constraints associated with the standard wear test procedures, a rather simple in-house sandpaper abrasion test procedure has been adopted in the present study to measure the wear/abrasion loss of wire-arc sprayed Zn-15Al coating in as-deposited conditions and after being cooled from elevated temperatures.

In the sandpaper abrasion test, the mechanical durability of the coating surface is evaluated under given applied stress when subjected to a certain number of abrasion cycles [42,43]. Specifically, in this paper, the Zn-15Al coating surface of size 5 cm x 5 cm was faced down onto 220-grit sandpaper of size 29.7 cm x 21 cm, and a test weight of 600 g was placed on the top surface of the specimen. The test setup applied normal stress of 3.3kPa for the considered load and contact area of the coating. The coating specimen with the test load on top was moved manually parallel to the long side of the sandpaper in one direction and turned 90 degrees and moved back along the long side on a new area of the sandpaper in the opposite direction. This moving cycle of back and forth was considered one abrasion cycle. See Fig. 4 for the schematic illustration of the abrasion test set-up. The sandpaper was replaced with a new one every 5 cycles to ensure all the specimens experienced similar abrasion. The weight of the specimens before the abrasion test and after 30 cycles of abrasion were recorded to calculate the coatings' wear/abrasion loss. The abrasion test was conducted on three specimens cooled down to room temperature from exposed

target elevated temperatures, and the corresponding wear loss (percentage) in the coating was calculated as follows.

$$\mu = \frac{(M_0 - M_a)}{M_0} X 100$$
 (Eq 2)

where, M_0 is the mass of the original coating and M_a is the mass of the coating after 30 cycles of abrasion.

Electrochemical Studies

The Zn-15Al coatings are widely used in various aggressive corrosive environments because of their reliable protection performance against substrate steel. Therefore, it is essential to characterize the electrochemical corrosion protection behavior of these coatings after being exposed to high temperatures. To this end, a non-destructive electrochemical technique [44-46] known as electrochemical impedance spectroscopy (EIS) was employed on the Zn-15Al coatings after being cooled from different target elevated temperatures to evaluate the changes in the electrochemical nature of the coating surface under open circuit potential (OCP). Corrosion is an electrochemical process in which electrons or ions move from one part of the metal (anode) to another (cathode) [47]. Therefore, the layers of materials in the corrosion system including the protective coating, electrolyte, and metal substrate can be modeled/ considered as a combination of (in parallel or series) elements in an electric circuit such as resistors and capacitors [48]. In brief, the behavior of the coating system mimics an electric circuit. Centered on this concept, in EIS the impedance (Z) of the corrosion system, which is the tendency to resist the flow of electrons through different layers of the corrosion system is measured over a wide range of frequencies Z(ω)

(Impedance as a function of frequency). Initially, an AC signal (with constant amplitude) at a very high frequency is applied to the system and as the experiment progresses, the frequency of the AC signal is slowly reduced. As frequencies of the AC signal change, different phenomena happen in the corrosion cell, such as migration or diffusion of ions through all layers of the corrosion system under study. Hence, by generating the impedance spectrum of the corrosion system $Z(\omega)$, one can derive insights into the corrosion behavior and kinetics of the coating [49]. In addition, the impedance of the system would change if there were a change in the coating conditions. In the present study, coating exposure to different elevated temperatures changed the coating's condition from its as-deposited state. Therefore, EIS was performed on Zn-15Al coatings using a threeelectrode electrochemical cell, where the test specimen (Zn-15Al coated steel plates) was configured as a working electrode (WE), platinum wire mesh as the counter electrode (CE), and saturated calomel electrode (SCE) as a reference electrode. The corrosion cell was placed in the Faraday cage to shield the electrochemical test setup from external interferences. The tests were performed on a 1 cm² working electrode area and 3.5 wt.% NaCl solution was used as an electrolyte. A Gamry potentiostat (Reference 600) was employed to carry out the tests. EIS measurements were taken by changing the frequency of the 3-mV(amplitude) sinusoidal voltage signal from 100 kHz to 0.01 Hz. A minimum of five replicates of Zn-15Al coatings were tested to ensure the repeatability of results. Please note that owing to the non-destructive nature of the EIS technique, no further morphological characterization of the coatings was conducted post-EIS.

Results and Discussion

The digital images of Zn-15Al coatings taken before exposure to elevated temperatures and after being cooled from exposed target elevated temperatures are presented in Fig. 5. Except for a slight discoloration, no apparent signs of delamination, and surface cracking/spalling of the

coating were noticed for coatings cooled from 600°C (see Fig. 5 (a) to (e)). Failure by surface cracking was observed in the coating when cooled from a temperature of 700°C as seen in Fig. 5 (f), and hence, higher temperatures are not investigated in this study. The coating failure by cracking at 700°C can be attributed to a combination of factors including stresses due to thermal expansion and thermal incompatibility between the substrate and coating, high-temperature oxidation, and phase changes that occurred in the coating microstructure. The detailed results from microstructural characterization tests, mechanical tests, and electrochemical tests are presented in this section of the manuscript.

SEM and EDS Analysis

The surface micrographs of the as-coated Zn-15Al coating and after cooling from elevated temperatures are provided in Fig. 6. These micrographs were taken at a magnification of 2500 X and at the same scale (10 μm) to make a fair comparison between coatings exposed to and cooled from different elevated temperatures. The as-coated surface of Zn-15Al coating appeared homogeneous (see Fig. 6 (a)). In addition, the XRD peaks acquired from the as-coated Zn-15Al coating show that the coating has only phases corresponding to pure zinc and pure aluminum (see Fig. 1 (b)). However, from Fig. 6 (b) to (d) it is evident that when cooled from 300°C, 400°C, and 500°C, new metallurgical phase formation occurred in the coating microstructure. The possible phases that can be expected for the Zn-15Al alloy exposed to high temperatures can be read from Zn-Al binary phase diagram provided in Fig. 3. These phase changes are noticeable on the SEM image taken on the Zn-15Al coating that was cooled from 400°C and very distinct from the Zn-15Al surface cooled from 500°C and can be seen in Fig. 6 (c) and (d). Therefore, EDS analysis was performed on these micrographs confirming the presence of three new phases including the eutectoid (α+η) phase which has a composition of 22 wt.% aluminum and 78 wt.% zinc. The other

two phases observed were partially converted eutectic ($\beta + \eta$), which consists of 89 wt.% zinc and 11 wt.% aluminum and zinc-rich η phase. The composition revealed from the EDS analysis in this study matched the corresponding phase composition reported in the literature [50]. Moreover, the microstructural arrangement of these phases revealed from the SEM image exhibited a peanut-shaped fine lamellar structure of eutectoid ($\alpha+\eta$) surrounded by the coarse lamellar structure of eutectic ($\eta+\beta$) in a lighter matrix of η phase. Similar microstructural changes were noticed in a study on the Zn-Al alloys as high-temperature lead-free solders [51]. The surface SEM of the Zn-15Al cooled from an exposed temperature of 600°C appeared to be heavily oxidized (see Fig. 6 (e)), and the corresponding cross-section shown in Fig. 7 (e) confirms it. Although no visible cracking was noticed on the surface of Zn-15Al coatings exposed to 600°C (see Fig. 5 (e)), coating deterioration in the microstructure was evident from the corresponding micrographs.

The SEM micrographs on the cross-sections of Zn-15Al coatings after being cooled from different target high temperatures are shown in Fig. 7. Unlike surface SEM images, phase changes were not obvious in the cross-section micrographs at the considered magnification. However, the increased porosity with an increase in the exposure temperature was evident from these micrographs. Although the uniform distribution of zinc and aluminum in the coating microstructure remained unaffected until 500°C, the appearance of the coating cross-section cooled from 600°C was different. A lighter grey matrix of material rich in zinc separated from the coating and deposited on the substrate steel and resembled galvanized steel, the remaining coating cross-section seems to contain a lot of voids, holes, and excessive oxides (see Fig. 7 (e)). In addition to the SEM images of the cross-sections, elemental maps of zinc, aluminum, and oxygen obtained from EDS analysis are provided in Fig. 8. As seen in Fig. 8 (a) to (d) the oxygen content increased substantially with an increase in the exposed temperature. Moreover, the presence of

increased porosity was apparent in these elemental maps too. The elemental maps of the cross-section after cooling from 600°C are not included in Fig. 8. Since the cross-section appeared haphazard, instead of elemental mapping, box EDS was performed on this cross-section, and the results are presented in Fig. 9. From the EDS spectra generated from the lighter matrix of material (marked "A" in Fig. 9) that was deposited on the substrate steel, it contains 70.00 wt.% of zinc, 20.60 wt.% oxygen, 6.88 wt.% iron, with only 0.57 wt.% of aluminum Fig. 9 (b). The separation of zinc from Zn-15Al alloy during exposure to 600°C can be attributed to the low melting point (420°C) and higher density of zinc (7.13 g/cm³) compared to aluminum (melting point - 660°C, density - 2.70 g/cm³). Further studies may be conducted to investigate the corrosion protection performance offered by this layer to substrate steel. On the other hand, the EDS spectra obtained from point B on the coating cross-section (see Fig. 9 (c)) revealed that the corresponding coating matrix was mainly composed of 33.00 wt.% oxygen, 22.00 wt.% aluminum, 20.00 wt.% zinc, and 19.00 wt.% iron. This confirms that the coating microstructure was heavily oxidized and damaged when exposed to 600°C.

Porosity Analysis

The average porosity value of Zn-15Al coating in the as-deposited condition was 6.47%. The porosity values increased with an increase in the target elevated temperature. The increased porosity values were 14.55%, 17.62%, and 23.68% in coating specimens cooled from 300°C, 400°C, and 500°C, respectively. The increase in porosity versus exposure temperature can be seen from the graph presented in Fig. 10. The consistent increase in porosity in Zn-15Al coating when cooled from different elevated temperatures can be attributed to high-temperature oxidation in the coating microstructure and thermal incompatibility between the substrate and the coating. Please note that the porosity analysis was not performed on the Zn-15Al coating cooled from 600°C due

to the incompatibility of the corresponding cross-section SEM image to run the analysis using ImageJ. However, there was a substantial increase in porosity in the coating cooled from 600°C due to the separation and deposition of zinc-rich matrix onto the substrate steel from the Zn-15Al alloy coating which can be observed in Fig. 7 (e).

X-ray Diffraction Analysis

The effect of high-temperature exposure on the Zn-15Al coatings deposited on steel substrates was characterized using XRD analysis. Fig. 11 (a) shows the XRD patterns of the asdeposited coating and coating after being cooled from 300°C exposure. The XRD patterns of asdeposited Zn-15Al and after exposure to 300°C were identical and comprised of peaks corresponding to pure aluminum and pure zinc. XRD spectra generated from Zn-15Al coatings cooled from 400°C and 500°C also had peaks corresponding to pure aluminum and zinc, similar to the as-deposited coatings. Additionally, Zn-15Al coatings cooled from 400°C, and 500°C also had SiO₂ (silica) peaks that could have been due to the trapping of polishing material in the porous microstructure of the cooled coating (see Fig. 11 (b)). Although the presence of zinc and aluminum oxidation products is expected after cooling from 400°C and 500°C, no corresponding peaks were noticed in the XRD spectra. It can be supposed that the oxide films formed on the coating surface after exposure to 400°C and 500°C are in an amorphous form and hence not detected by XRD [52]. Finally, the XRD spectra of the Zn-15Al coatings cooled from 600°C consisted of peaks corresponding to zinc oxide (ZnO), corundum (Al₂O₃), silica (SiO₂), and zinc aluminum hydroxide carbonate hydrate (Zn_{0.66}Al_{0.34}(OH)₂(CO₃)_{0.17}(H₂O)_{0.7}) along with the peaks of pure zinc and pure aluminum phases, as seen in Fig. 11 (c). This XRD pattern confirms the extent of deterioration in the Zn-15Al coating microstructure when exposed to 600°C and agrees with the inferences drawn from the SEM images of the coating discussed previously in the section SEM and EDS Analysis.

The effect of the microstructural changes on the coating's mechanical integrity and electrochemical corrosion behavior is discussed in the following sections.

Vickers Microhardness

Vickers microhardness test was performed using the protocols described in the section Mechanical Properties Evaluation to quantify the changes in the mechanical properties of postfire Zn-15Al coatings cooled from temperatures up to 600°C. The average values of HV obtained from 15 indentations made on the random regions of the coating cross-sections cooled from exposure to different elevated temperatures are presented in Fig. 12. The plot indicated an increasing trend in the HV value of the coating with an increase in exposed temperatures up to 500°C, and a sudden decrease in HV value was noticed in the coatings exposed to 600°C. The average HV value for Zn-15Al coating in the as-deposited condition was 32.56 HV, and this is in line with the values reported in the literature [53]. The increase in post-fire coating's hardness value, when exposed to temperatures up to 500°C, can be attributed to the partial transformation of the amorphous phase of the coating into a nanocrystalline structure, which disperses in the coating and hardens it [54]. Moreover, the presence of closely spaced lamella of eutectic ($\eta + \beta$), and eutectoid $(\alpha+\eta)$ phases were observed in the coating microstructure (see Fig. 6 (c) and (d)). These intermetallic phases are described as hard and brittle in literature [51]. Therefore, the formation of these phases is reflected as the increase in microhardness of the coating with an increase in the target elevated temperature during the Vickers hardness test. On the other hand, the decrease in hardness value to 18.68 HV at 600°C can be attributed to the increased porosity and oxidation in the coating microstructure confirmed by the SEM micrographs of the coating presented in Fig. 6 (e), Fig. 7 (e) and from XRD results presented in Fig. 11 (c). In short, the results

of the Vickers microhardness test reiterate the deterioration in the Zn-15Al coating microstructure when exposed and cooled from 600°C.

Wear loss measurements

Abrasion test results of Zn-15Al coating measured using sandpaper abrasion test described in the section Mechanical Properties Evaluation are presented in Fig. 13. A nominal wear loss (<3%) was observed in coatings until cooled from an exposure temperature of 400°C and an increase (~10 times or 22 wt.%) in the wear loss was noticed in coatings cooled from 500°C. This increase in wear loss at this temperature can be due to the brittle nature of the intermetallic phases formed and oxidation products in the coating microstructure. On the other hand, a substantial increase in wear loss was evident in the coatings cooled from 600°C, where approximately 45% of the coating was abraded. This can be attributed to the high-temperature oxidation which resulted in the formation of various oxidation products of zinc and aluminum when subjected to 600°C. According to the diffraction peaks generated from the Zn-15Al coating exposed to and cooled from 600°C, the coating microstructure consisted of oxidation products including ZnO, Al₂O₃, and zincaluminum carbonate hydroxide (see Fig. 11 (c)). The vulnerability of these oxidation products to abrasion/wear manifested in the abrasion results of Zn-15Al coatings subjected to 600°C. Although no noticeable surface cracks appeared on the surface of the Zn-15Al coatings after exposure and cooling from 600°C, (refer to the image provided in Fig. 5 (e)), the results of the microstructural characterization and mechanical tests demonstrate that the coating microstructure had deteriorated and compromised its mechanical integrity when cooled from this temperature. Therefore, no further corrosion testing was performed on the Zn-15Al coatings that were cooled from 600°C. The following sections elucidate the results obtained from the electrochemical testing of Zn-15Al coatings after exposure to elevated temperatures up to 500°C.

Electrochemical Impedance Spectroscopy

EIS test was performed using the protocols described in the section **Electrochemical Studies** to infer the changes in electrochemical corrosion behavior of the Zn-15Al coating after being cooled from different elevated temperatures. As mentioned previously in **Electrochemical Studies**, during EIS we measure the impedance (resistance) of the system under study[48]. Since the impedance of the system is a complex number it consists of real and imaginary components typically presented using a Nyquist plot [55]. Thus, the Nyquist plot is a complex-impedance plane representation of the system at each frequency point where the imaginary component of the impedance is plotted on the Y-axis versus the real part of the impedance on the X-axis. The generated Nyquist plot can be interpreted either based on physical intuition from the system and/or by fitting the EIS data using an equivalent electrical circuit (EEC) [56]. The Nyquist plots obtained from the Zn-15Al coatings after being cooled from different elevated temperatures are shown in Fig. 14.

In the Nyquist plot, the point where the impedance spectrum meets the X-axis at higher frequencies (beginning of the semi-circle loop, where imaginary Z is zero) is called solution resistance (R_s), which is related to the transport properties of the electrolyte [57]. The location where the impedance spectrum meets the X-axis at low frequencies (imaginary Z is zero again), is called charge transfer resistance and is often represented using R_{ct}. Charge transfer resistance is a measure of the difficulty encountered when an ion or electron is moving through the coating. In the Nyquist plot, the charge transfer resistance is represented as the diameter of the semicircle [58]. Therefore, the larger the semi-circle loop, the higher the charge transfer resistance of the system which indicates higher impedance/resistance offered by the coating (working electrode) to the flow of ions through it. In the present study, although, the coating exhibited an identical behavior

(showing a single semi-circle loop) after being cooled from each of the elevated temperatures including 300°C, 400°C, and 500°C, the diameter of the semi-circle increased with an increase in the exposure temperature. Since the larger diameters correspond to higher charge transfer resistance it indicates better corrosion protection from the surface that encounters the corrosive medium [10]. In the case of Zn-15Al coating, this behavior can be attributed to the melting and rearrangement of metals in the microstructure and the formation of oxidation products. Since metal oxides have a higher impedance than metals it is reflected in the increased impedance of the coating surface with the increase in exposure temperature until 500°C.

Although the Nyquist plot provides information about changes in the system's impedance and helps read important parameters such as solution resistance (R_s) and charge transfer resistance (R_{ct}) directly, the frequency information is not visible in that plot. Another representation of the data obtained from the EIS study is called the Bode plot which presents information about the changes in impedance (Z) and phase shift (°) over the entire range of frequencies. On the Bode plots, The X-axis is a logarithmic scale of the frequency, and the Y-axis is either the logarithm of the modulus of impedance Z or the phase shift (see Fig. 15 and Fig. 16). From the Bode modulus frequency plot shown in Fig. 15, the impedance values obtained for Zn-15Al coating were 280.5 Ω -cm², 645.0 Ω -cm², 804.8 Ω -cm², and 819.6 Ω -cm², as-deposited condition, and after being cooled from 300°C, 400°C, and 500°C, respectively, indicating that the top surface of the Zn-15Al coating has become more resistant to corrosive medium when exposed target elevated temperatures and this can be attributed to the increased formation of the high-temperature oxidation products in the coating microstructure that hinders the movement of ions. Despite an increase in porosity with exposure temperature, the coating's impedance values were not adversely affected. The observed increase in impedance could be explained by the greater surface of the

porous coating structure after exposure to elevated temperatures, which could have provided more active sites for the formation of high-temperature oxidation products that blocked the corrosive medium to pass through [59,60]. Additionally, the microstructure of the coating after high-temperature exposure consisted of defects such as globular pores that were not connected to the upper surface of the coating, resulting in closed rather than open pores [61]. However, in order to mitigate corrosion effectively, prolong the service life, and avoid accidental corrosion through any interconnected pores, it is important to apply suitable sealing treatments to the fire-exposed Zn-15Al coatings before reusing them.

In the Bode phase angle frequency plot (see Fig. 16), only one phase angle peak was observed for Zn-15Al coatings cooled from all the exposed temperatures, which qualitatively signifies that the system had one RC time constant [62]. In other words, there is only one RC circuit (a resistor and a capacitor in parallel) is present in the system under study. The phase angle peak from the coating in as-deposited condition appeared between 0.01 and 0.1 Hz and the phase angle peak shifted to higher studied frequencies after exposing the coating to different elevated temperatures and it is due to the formation of oxidation products on the coating surface. Although, a slight reduction in phase angle peak was observed from Zn-15Al coatings cooled from 400°C and 500°C the peak stayed within 5° when compared to the as-deposited condition of the coating. The higher phase angle at a higher studied frequency also reflects the protective nature of the surface in contact with the electrolyte [63]. Therefore, the results of the EIS studies on the post-fire Zn-15Al coatings indicate that even after being subjected to different elevated temperatures, the Zn-15Al coating still offers corrosion protection to the substrate steel from the chloride environment until 500°C.

Conclusions

In this paper, the post-fire behaviors of the wire arc sprayed Zn-15Al coatings were studied, with emphasis on the changes in the microstructural, mechanical, and electrochemical corrosion properties, to assess the residual performance and integrity of the coating. The key findings are summarized as follows:

- (1) The coating survived temperature exposure up to 600°C with no apparent defects/cracks noticed until this temperature except for little discoloration. But the coating failed by cracking when subjected to and cooled from 700°C.
- (2) SEM and EDS analysis performed on the Zn-15Al coating revealed various changes in the coating's microstructure when exposed to different elevated temperatures. The formation of intermetallic phases of zinc and aluminum was noticed on the SEM micrographs of the coating's surface cooled from an exposure temperature of 400°C and 500°C. The intermetallic phases observed were eutectoid (α+η) with a composition of 22 wt.% aluminum and 78 wt.% zinc, partially converted eutectic (β+η) with a composition of 89 wt.% zinc and 11 wt.% aluminum and a zinc-rich η-phase. Separation of the zinc-rich matrix was identified in the cross-section micrographs of the coating cooled from 600°C and the corresponding surface micrograph also appeared heavily oxidized.
- (3) XRD study confirmed the formation of various oxidation products on the coating that was cooled from 600°C such as zinc oxide (ZnO), corundum (Al₂O₃), silica (SiO₂), and zinc aluminum hydroxide carbonate hydrate (Zn_{0.66}Al_{0.34}(OH)₂(CO₃)_{0.17}(H₂O)_{0.7}) along with the peaks of pure zinc and pure aluminum phases. This diffraction pattern agrees with the observations made from the SEM imaging and EDS analysis.

- (4) The porosity analysis performed on the cross-section micrographs of the Zn-15Al coating after exposure to each of the target elevated temperatures showed that the porosity in the coating microstructure increased (~ 3.7 times) from 6.47% in as-deposited conditions to 23.68% after being cooled from 500°C. The increased porosity can be attributed to the increased oxidation in the coating with the increase in exposure temperature.
- (5) The Vickers microhardness of the coating increased from 32.56 HV to 43.7 HV when the exposed temperature increased from room temperature to 500°C due to the formation of harder intermetallic phases. On the other hand, the HV value was reduced to 18.68 HV on the surface of the coating cooled from an exposure temperature of 600°C resulting from the increased oxidation and deterioration in the coating microstructure and it agrees with the results obtained from the aforementioned characterization tests.
- (6) The wear/ abrasion resistance of the coating remains unaffected up to 400°C and the coating exhibited a wear loss of < 3%. However, the wear loss increased to 22.23% and 45.62% in coatings subjected to and cooled from temperatures 500°C and 600°C respectively. The increase in wear loss at 500°C can be attributed to the brittle nature of phases formed and the substantial increase at 600°C reiterates the coating's increased oxidation that leads to increased vulnerability to abrasion.
- (7) The EIS studies performed on the coating revealed that the coating surface exhibited increased corrosion resistance with the increase in the exposure temperature and the impedance values increased from 280.5 Ω -cm² in as-deposited conditions to 645.0 Ω -cm², 804.8 Ω -cm², and 819.6 Ω -cm² after being cooled from 300°C, 400°C, and 500°C exposure. This can be attributed to the melting and re-arrangement of coating microstructure and the presence of high-

temperature oxidation products. However, to mitigate porosity, it is recommended to properly seal fire-exposed Zn-15Al coated steels prior to reuse.

Thus, the microstructural characterization, mechanical integrity tests, and electrochemical studies confirm the uncompromised performance of wire-arc sprayed Zn-15Al coatings after being subjected to different elevated temperatures up to 500°C and deterioration when subjected to a temperature of 600°C and above. In the future, a detailed study on the long-term performance of the post-fire Zn-15Al coatings with different exposure conditions such as immersion and salt spray can be conducted to comprehend the long-term corrosion protection offered by these fire-exposed Zn-1 5Al coated steels. In addition, this study can be extended to other commonly used thermally sprayed anti-corrosive coatings such as pure zinc, pure aluminum, and other alloy compositions of zinc-aluminum to evaluate their residual service life after being subjected to high fire temperatures.

CRediT authorship contribution statement

Ratna Yasoda: Data curation, Methodology, Formal analysis, Investigation, Writing - original draft, Writing - review & editing. Ying Huang: Project administration, Funding acquisition, Methodology, Supervision, Writing - review & editing. Ravi Kiran: Methodology, Writing - review & editing. Xiaoning Qi: Investigation, Writing -review & editing.

Acknowledgments

This work was supported by the National Science Foundation under Grant No. CMMI-1750316 and OIA-2119691. The findings and opinions expressed in this article are those of the authors only and do not necessarily reflect the views of the sponsors.

References

- 1. S. Brito, I. Bastos, H. Costa, Corrosion resistance and characterization of metallic coatings deposited by thermal spray on carbon steel, *Materials & Design*, **41**, 282-288 (2012)
- 2. P.L. Fauchais, J.V. Heberlein, M.I. Boulos, Thermal spray fundamentals: from powder to part, Springer Science & Business Media, 2014
- 3. H. Katayama, S. Kuroda, Long-term atmospheric corrosion properties of thermally sprayed Zn, Al and Zn–Al coatings exposed in a coastal area, *Corrosion Science*, **76**, 35-41 (2013)
- 4. A. Darabi, F. Azarmi, Investigation on Relationship Between Microstructural Characteristics and Mechanical Properties of Wire-Arc-Sprayed Zn-Al Coating, *Journal of Thermal Spray Technology*, **29**(1-2), 297-307 (2020)
- 5. G. Jandin, H. Liao, Z. Feng, C. Coddet, Correlations between operating conditions, microstructure and mechanical properties of twin wire arc sprayed steel coatings, *Materials Science and Engineering: A*, **349**(1-2), 298-305 (2003)
- 6. T.-Y. Yung, T.-C. Chen, K.-C. Tsai, W.-F. Lu, J.-Y. Huang, T.-Y. Liu, Thermal spray coatings of Al, ZnAl and inconel 625 alloys on SS304L for anti-saline corrosion, *Coatings*, **9**(1), 32 (2019)
- Z. Panossian, L. Mariaca, M. Morcillo, S. Flores, J. Rocha, J. Pena, F. Herrera, F. Corvo,
 M. Sanchez, O. Rincon, Steel cathodic protection afforded by zinc, aluminium and zinc/aluminium alloy coatings in the atmosphere, *Surface and Coatings Technology*, 190(2-3), 244-248 (2005)
- 8. A. Gulec, O. Cevher, A. Turk, F. Ustel, F. Yilmaz, Accelerated corrosion behaviors of Zn, Al and Zn/15Al coatings on a steel surface, *Materiali in tehnologije*, **45**(5), 477-482 (2011)

- 9. R.D. Yasoda, Y. Huang, X. Qi, Corrosion Performance of Wire Arc Deposited Zinc Aluminum Pseudo Alloy and Zinc 15 Aluminum Alloy Coatings on Steel in Chloride Environment, *Journal of Thermal Spray Technology*, 1-16 (2022)
- 10. H.-S. Lee, J.K. Singh, M.A. Ismail, C. Bhattacharya, A.H. Seikh, N. Alharthi, R.R. Hussain, Corrosion mechanism and kinetics of Al-Zn coating deposited by arc thermal spraying process in saline solution at prolong exposure periods, *Scientific reports*, **9**(1), 1-17 (2019)
- 11. Y.-t. Li, B.-r. Hou, Anticorrosion Mechanism of Thermal Spraying Coatings of Zinc and Aluminum and of Alloys Made of the Same in Marine Environment: A Review, *MATERIALS PROTECTION-WUHAN-*, **38**(9), 30 (2005)
- 12. A.R. Moreira, Z. Panossian, P.L. Camargo, M.F. Moreira, I.C.d. Silva, J.E.R. de Carvalho, Zn/55Al coating microstructure and corrosion mechanism, *Corrosion Science*, **48**(3), 564-576 (2006)
- 13. S.-j. Tong, Z.-z. Wu, R.-j. Wang, H. Wu, Fire risk study of long-distance oil and gas pipeline based on QRA, *Procedia Engineering*, **135**, 369-375 (2016)
- 14. X. Li, F. Khan, M. Yang, C. Chen, G. Chen, Risk assessment of offshore fire accidents caused by subsea gas release, *Applied Ocean Research*, **115**, 102828 (2021)
- 15. C. Lam, W. Zhou, Statistical analyses of incidents on onshore gas transmission pipelines based on PHMSA database, *International Journal of Pressure Vessels and Piping*, **145**, 29-40 (2016)
- 16. M. Garlock, I. Paya-Zaforteza, V. Kodur, L. Gu, Fire hazard in bridges: Review, assessment and repair strategies, *Engineering structures*, **35**, 89-98 (2012)

- 17. S.E. Quiel, T. Yokoyama, L.S. Bregman, K.A. Mueller, S.M. Marjanishvili, A streamlined framework for calculating the response of steel-supported bridges to open-air tanker truck fires, *Fire Safety Journal*, **73**, 63-75 (2015)
- 18. S.S. Schulze, E.C. Fischer, S. Hamideh, H. Mahmoud, Wildfire impacts on schools and hospitals following the 2018 California Camp Fire, *Natural Hazards*, **104**(1), 901-925 (2020)
- 19. P.J. Camilleri, C. Healy, E.M. Macdonald, S. Nicholls, J. Sykes, G. Winkworth, M. Woodward, Recovery from bushfires: The experience of the 2003 Canberra bushfires three years after, (2010)
- 20. N. Habermann, R. Hedel, Damage functions for transport infrastructure, *International* journal of disaster resilience in the built environment, **9**(4/5), 420-434 (2018)
- 21. V. Kodur, M. Naser, Fire hazard in transportation infrastructure: Review, assessment, and mitigation strategies, *Frontiers of Structural and Civil Engineering*, **15**(1), 46-60 (2021)
- R. Chijiiwa, Y. Yoshida, R. Uemori, H. Tamehiro, K. Funato, Y. Horii, Development and practical application of fire-resistant steel for buildings, Nippon steel technical reported., Publ by Nippon Steel Corp, 1993, p 47-55
- M. Jimenez, S. Duquesne, S. Bourbigot, Multiscale experimental approach for developing high-performance intumescent coatings, *Industrial & engineering chemistry research*,
 45(13), 4500-4508 (2006)
- 24. H.U. Sajid, R. Kiran, Post-fire mechanical behavior of ASTM A572 steels subjected to high stress triaxialities, *Engineering Structures*, **191**, 323-342 (2019)

- H.U. Sajid, D.L. Naik, R. Kiran, Microstructure–Mechanical Property Relationships for Post-Fire Structural Steels, *Journal of Materials in Civil Engineering*, 32(6), 04020133 (2020)
- 26. X. Qiang, F.S. Bijlaard, H. Kolstein, Post-fire mechanical properties of high strength structural steels S460 and S690, *Engineering Structures*, **35**, 1-10 (2012)
- 27. X. Qiang, F.S. Bijlaard, H. Kolstein, Post-fire performance of very high strength steel S960, *Journal of Constructional Steel Research*, **80**, 235-242 (2013)
- 28. M.A. Alam, E.-S.M. Sherif, S.M. Al-Zahrani, Fabrication of various epoxy coatings for offshore applications and evaluating their mechanical properties and corrosion behavior, *Int. J. Electrochem. Sci*, **8**, 3121-3131 (2013)
- 29. J.P. Ault, The use of coatings for corrosion control on offshore oil structures, *Journal of protective coatings & linings*, **23**(4), 42-46 (2006)
- 30. P. Fauchais, A. Vardelle, Thermal sprayed coatings used against corrosion and corrosive wear, *Advanced plasma spray applications*, **10**, 34448 (2012)
- 31. M. Bajpai, V. Shukla, F. Habib, Development of a heat resistant UV-curable epoxy coating, *Progress in organic coatings*, **53**(4), 239-245 (2005)
- 32. A. Buch, Pure metals properties: a scientific and technical handbook, (1999)
- 33. M. William, G.P. J, S.A. M, Performance of Protective Coatings on Small Steel Bridges Subject to Bushfires, 8th Australian Small Bridge Conferenceed., 2017, p 1 to 25
- 34. R.C. Tucker, Thermal spray technology, *ASM Handbook*, **5**, (2013)
- 35. H.U. Sajid, R. Kiran, Influence of stress concentration and cooling methods on post-fire mechanical behavior of ASTM A36 steels, *Construction and Building Materials*, **186**, 920-945 (2018)

- 36. W. Wang, T. Liu, J. Liu, Experimental study on post-fire mechanical properties of high strength Q460 steel, *Journal of Constructional Steel Research*, **114**, 100-109 (2015)
- 37. K. Geels, D.B. Fowler, W.-U. Kopp, M.R. ckert, Metallographic and materialographic specimen preparation, light microscopy, image analysis, and hardness testing, ASTM international West Conshohocken, 2007
- 38. M. Federici, G. Straffelini, S. Gialanella, Pin-on-disc testing of low-metallic friction material sliding against HVOF coated cast iron: modelling of the contact temperature evolution, *Tribology Letters*, **65**(4), 1-12 (2017)
- 39. S. Ahmad, A. Gupta, E. Sharmin, M. Alam, S. Pandey, Synthesis, characterization and development of high performance siloxane-modified epoxy paints, *Progress in organic coatings*, **54**(3), 248-255 (2005)
- 40. ASTM G99, Standard Test Method for Wear Testing with a Pin-on-Disk Apparatus,

 Annual Book of ASTM Standards, 3, 401 (1999)
- 41. M. Morgeneyer, N. Shandilya, Y.-M. Chen, O. Le Bihan, Use of a modified Taber abrasion apparatus for investigating the complete stress state during abrasion and in-process wear particle aerosol generation, *Chemical Engineering Research and Design*, **93**, 251-256 (2015)
- 42. M. Li, Y. Li, F. Xue, X. Jing, A robust and versatile superhydrophobic coating: Wear-resistance study upon sandpaper abrasion, *Applied Surface Science*, **480**, 738-748 (2019)
- 43. J.-H. Zhi, L.-Z. Zhang, Y. Yan, J. Zhu, Mechanical durability of superhydrophobic surfaces: The role of surface modification technologies, *Applied Surface Science*, **392**, 286-296 (2017)

- 44. M.S. Koochaki, R.E. Neisiany, S.N. Khorasani, A. Ashrafi, S.P. Trasatti, M. Magni, The influence of the healing agent characteristics on the healing performance of epoxy coatings: Assessment of the repair process by EIS technique, *Progress in Organic Coatings*, 159, 106431 (2021)
- 45. L.A. Middlemiss, A.J. Rennie, R. Sayers, A.R. West, Characterisation of batteries by electrochemical impedance spectroscopy, *Energy Reports*, **6**, 232-241 (2020)
- 46. A. Ejbouh, A. Ech-chebab, S. Hassi, M. Galai, H. Benqlilou, M.E. Touhami, Durability assessment of LC3-based reinforced concrete under combined chloride-sulfate environment via the EIS technique, *Construction and Building Materials*, **366**, 130194 (2023)
- 47. S.W. Dean Jr, Electrochemical methods of corrosion testing, *Paper*, (113), (1976)
- 48. M.E. Orazem, B. Tribollet, Electrochemical impedance spectroscopy, *New Jersey*, 383-389 (2008)
- 49. F. Ciucci, Modeling electrochemical impedance spectroscopy, *Current Opinion in Electrochemistry*, **13**, 132-139 (2019)
- 50. M. Demirtas, G. Purcek, H. Yanar, Z. Zhang, Z. Zhang, Effect of chemical composition and grain size on RT superplasticity of Zn-Al alloys processed by ECAP, *Letters on materials*, **5**(3), 328-334 (2015)
- 51. M.M. Hasan, A. Sharif, M.A. Gafur, Characteristics of eutectic and near-eutectic Zn–Al alloys as high-temperature lead-free solders, *Journal of Materials Science: Materials in Electronics*, **31**(2), 1691-1702 (2020)

- 52. T. Polcar, A. Cavaleiro, High temperature properties of CrAlN, CrAlSiN and AlCrSiN coatings–Structure and oxidation, *Materials Chemistry and Physics*, **129**(1-2), 195-201 (2011)
- 53. T.-C. Chen, C.-C. Chou, T.-Y. Yung, K.-C. Tsai, J.-Y. Huang, Wear behavior of thermally sprayed Zn/15Al, Al and Inconel 625 coatings on carbon steel, *Surface and Coatings Technology*, **303**, 78-85 (2016)
- 54. S. Liu, Y. Zhu, X. Lai, X. Zheng, R. Jia, X. Yuan, Influence of different heat treatment temperatures on the microstructure, corrosion, and mechanical properties behavior of Febased amorphous/nanocrystalline coatings, *Coatings*, **9**(12), 858 (2019)
- 55. B.-A. Mei, O. Munteshari, J. Lau, B. Dunn, L. Pilon, Physical interpretations of Nyquist plots for EDLC electrodes and devices, *The Journal of Physical Chemistry C*, **122**(1), 194-206 (2018)
- 56. B.-A. Mei, J. Lau, T. Lin, S.H. Tolbert, B.S. Dunn, L. Pilon, Physical interpretations of electrochemical impedance spectroscopy of redox active electrodes for electrical energy storage, *The Journal of Physical Chemistry C*, **122**(43), 24499-24511 (2018)
- 57. I. Margarit-Mattos, EIS and organic coatings performance: Revisiting some key points, *Electrochimica Acta*, **354**, 136725 (2020)
- 58. Y. Chen, W. Jepson, EIS measurement for corrosion monitoring under multiphase flow conditions, *Electrochimica Acta*, **44**(24), 4453-4464 (1999)
- 59. Z. Wang, J. Zhang, X. Liu, J. Liu, G. Liu, Failure mechanism of plasma sprayed Tb-YSZ coating under NaCl high-low temperature cyclic corrosion, *Surface and Coatings Technology*, 129244 (2023)

- 60. G. Binal, Isothermal oxidation and hot corrosion behavior of HVOF sprayed 80Ni-20Cr coatings at 750° C, *Surface and Coatings Technology*, **454**, 129141 (2023)
- 61. J.G. Odhiambo, W. Li, Y. Zhao, C. Li, Porosity and its significance in plasma-sprayed coatings, *Coatings*, **9**(7), 460 (2019)
- 62. F. Mansfeld, C. Tsai, Determination of coating deterioration with EIS: I. Basic relationships, *Corrosion*, **47**(12), 958-963 (1991)
- 63. P. Rodič, I. Milošev, Electrochemical and salt spray testing of hybrid coatings based on Si and Zr deposited on Aluminum and its alloys, *Journal of The Electrochemical Society*, **162**(10), C592 (2015)
- 64. A. Pola, M. Tocci, F.E. Goodwin, Review of microstructures and properties of zinc alloys, *Metals*, **10**(2), 253 (2020)

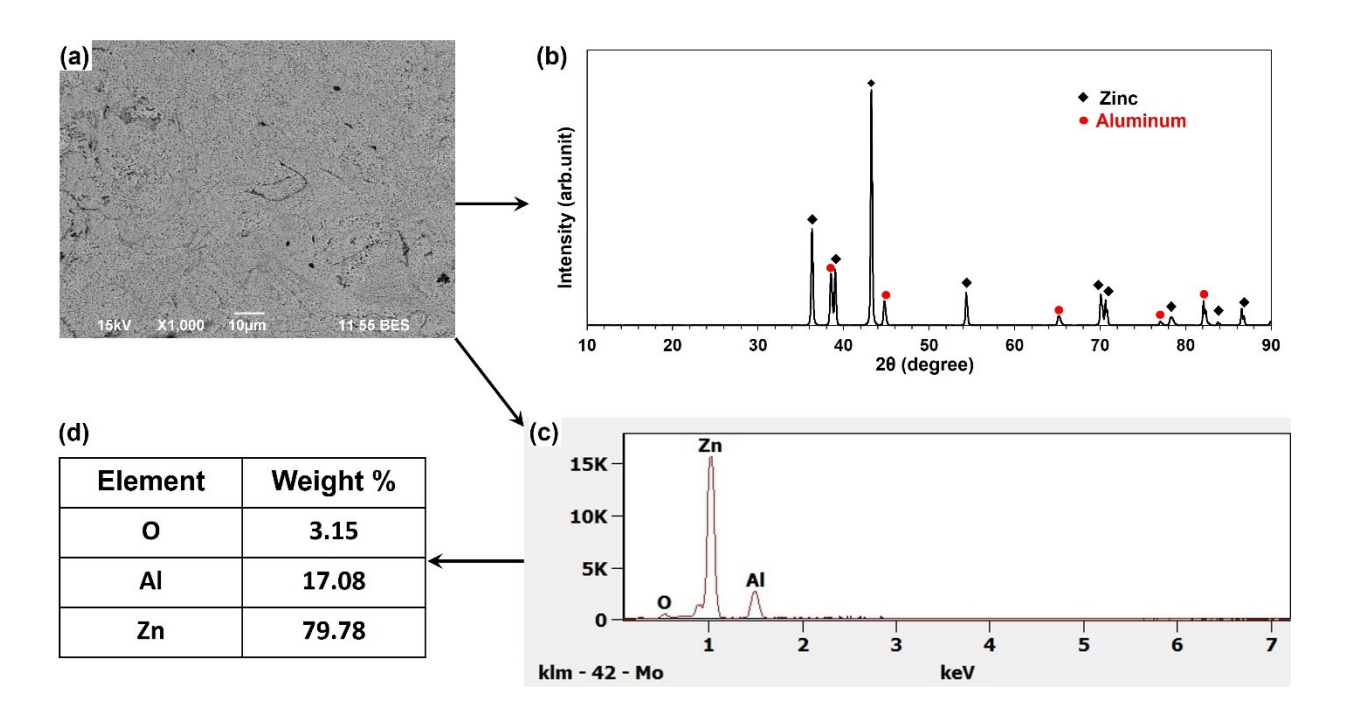


Fig. 1 Zn-15Al coating: a) surface SEM image b) XRD pattern c) EDS map and d) chemical composition from EDS in as-deposited conditions showing the superior quality of the produced coating using the wire-arc spray process

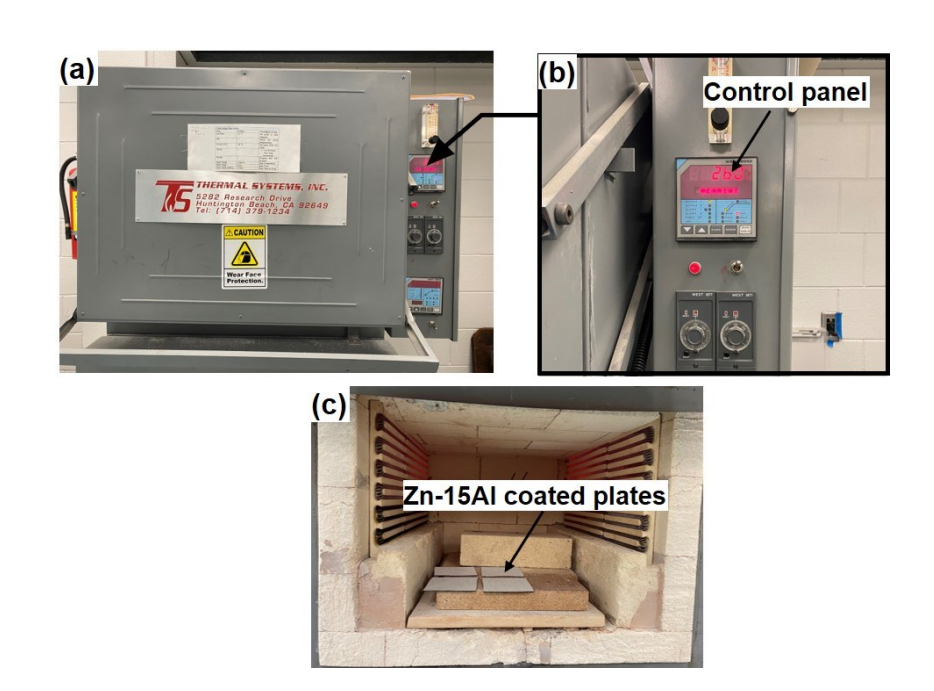


Fig. 2 Electric furnace a) exterior view, b) control panel, c) interior view with Zn-15Al coated steel plates on the fire bricks

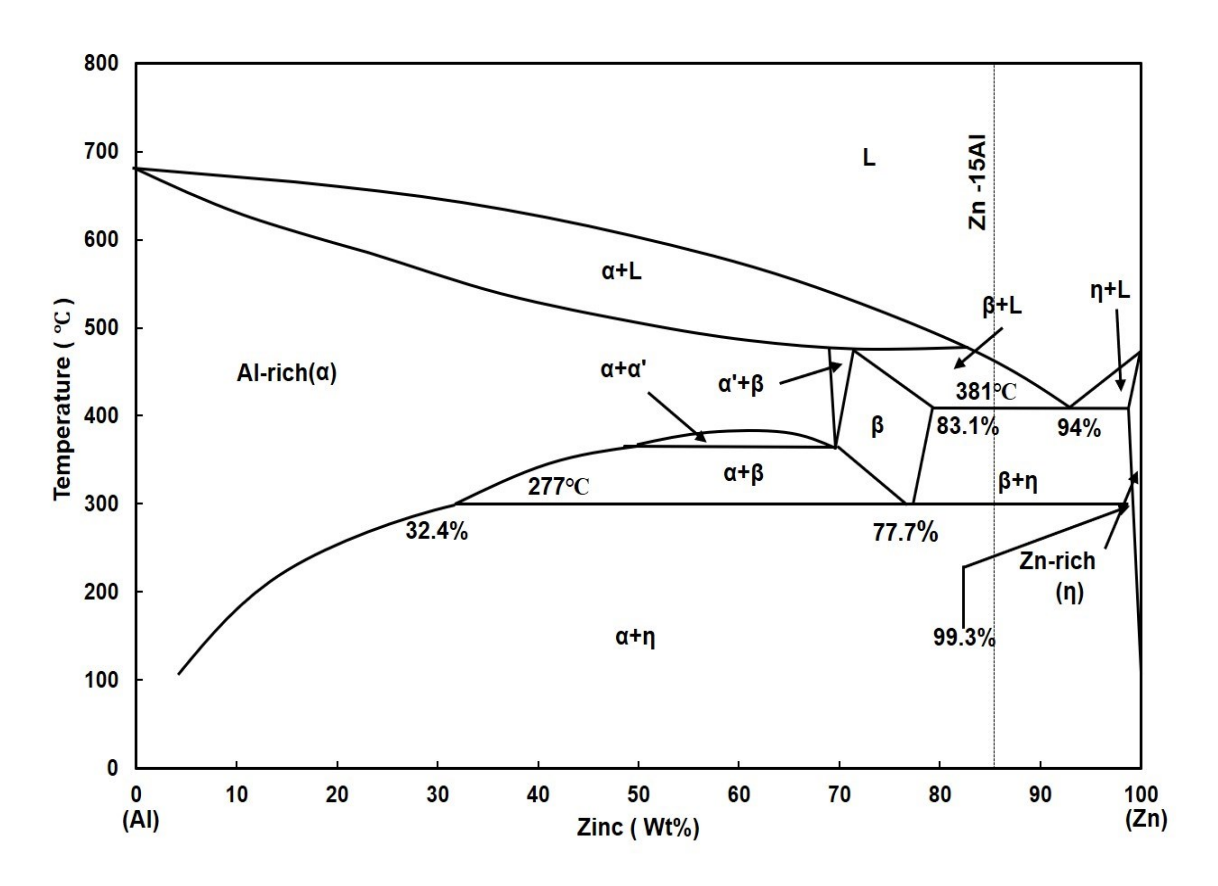


Fig. 3 Zinc-Aluminum phase diagram adopted from [64]

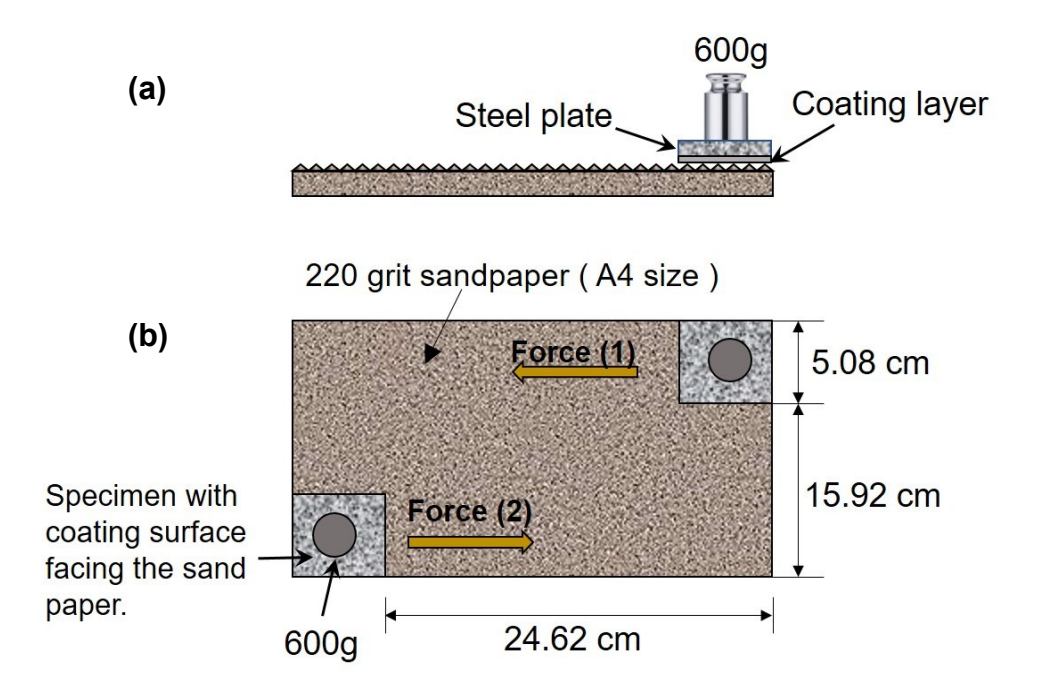


Fig. 4 Schematic illustration of the abrasion test showing (a) side view of the test set up, and (b) top view of the test set up showing the details and the directions of force (1) and force (2) which together complete one abrasion cycle

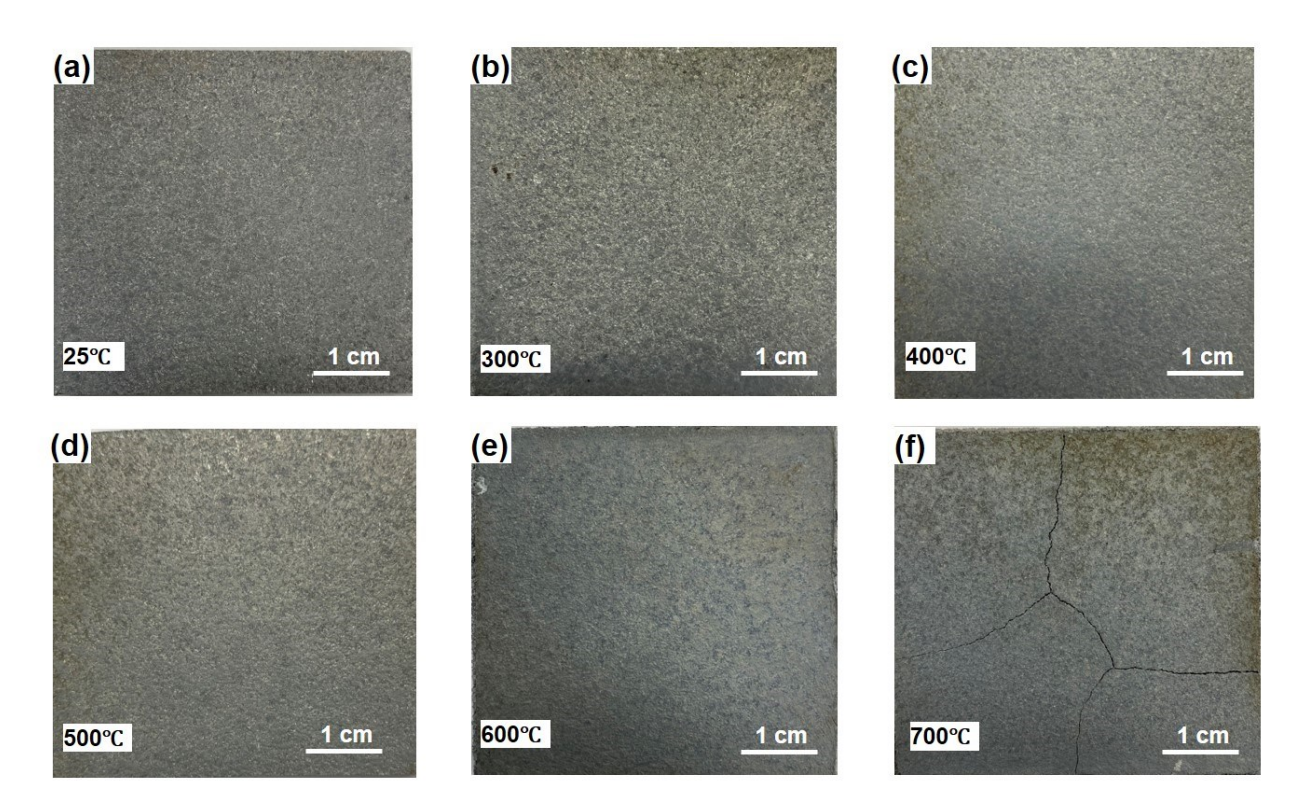


Fig. 5 Visual appearance of Zn-15Al coating surface a) at 25°C (in as-deposited condition), and after cooling from b) 300°C, c) 400°C, d) 500°C, e) 600°C, and f) 700°C

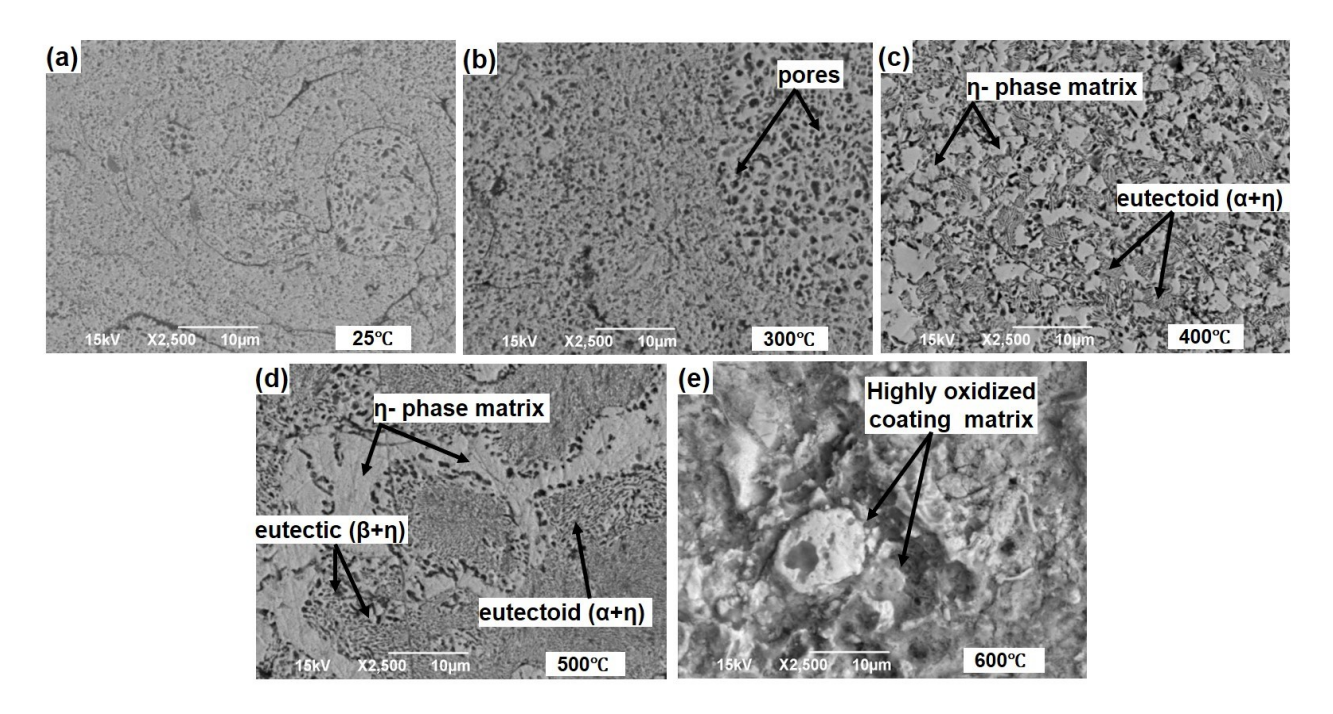


Fig. 6 SEM images on the surface of Zn-15Al coatings at a) 25°C (in as-deposited condition) and after cooling from b) 300°C, c) 400°C, d) 500°C, and e) 600°C showing corresponding changes in the morphology and microstructural features

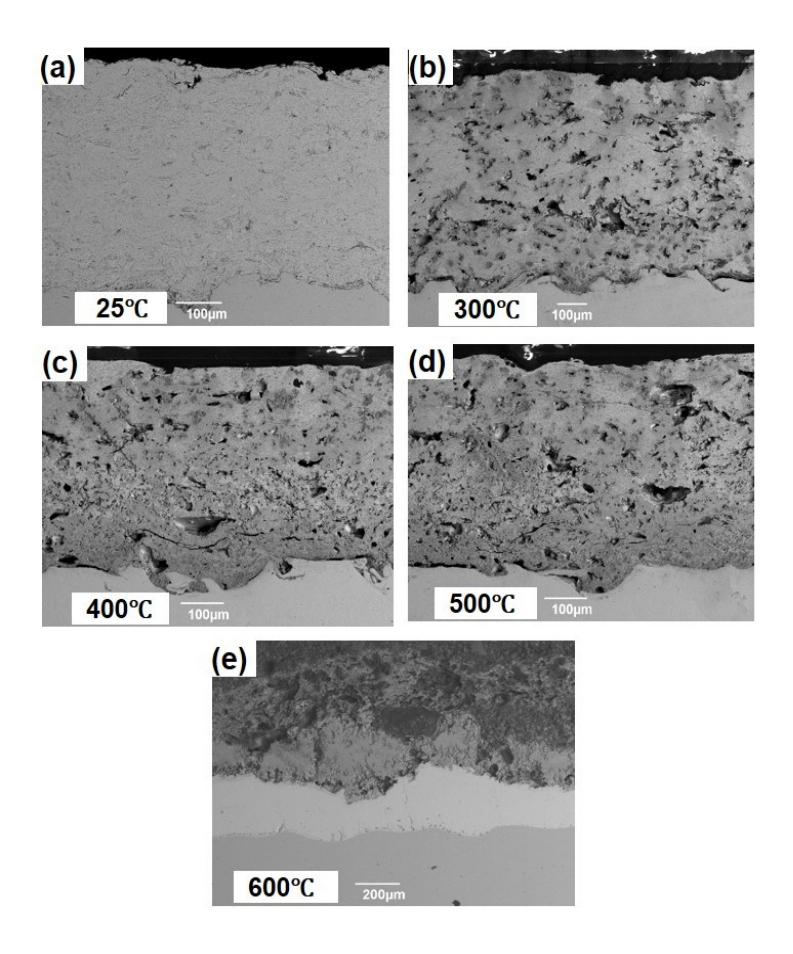


Fig. 7 SEM images on the cross-section of Zn-15Al coatings at a) 25°C (in as-deposited condition) and after cooling from b) 300°C, c) 400°C, d) 500°C, and e) 600°C. These images reveal the increase in porosity with an increase in exposure temperature and separation of the alloyed coating into two distinct phases after cooling from 600°C

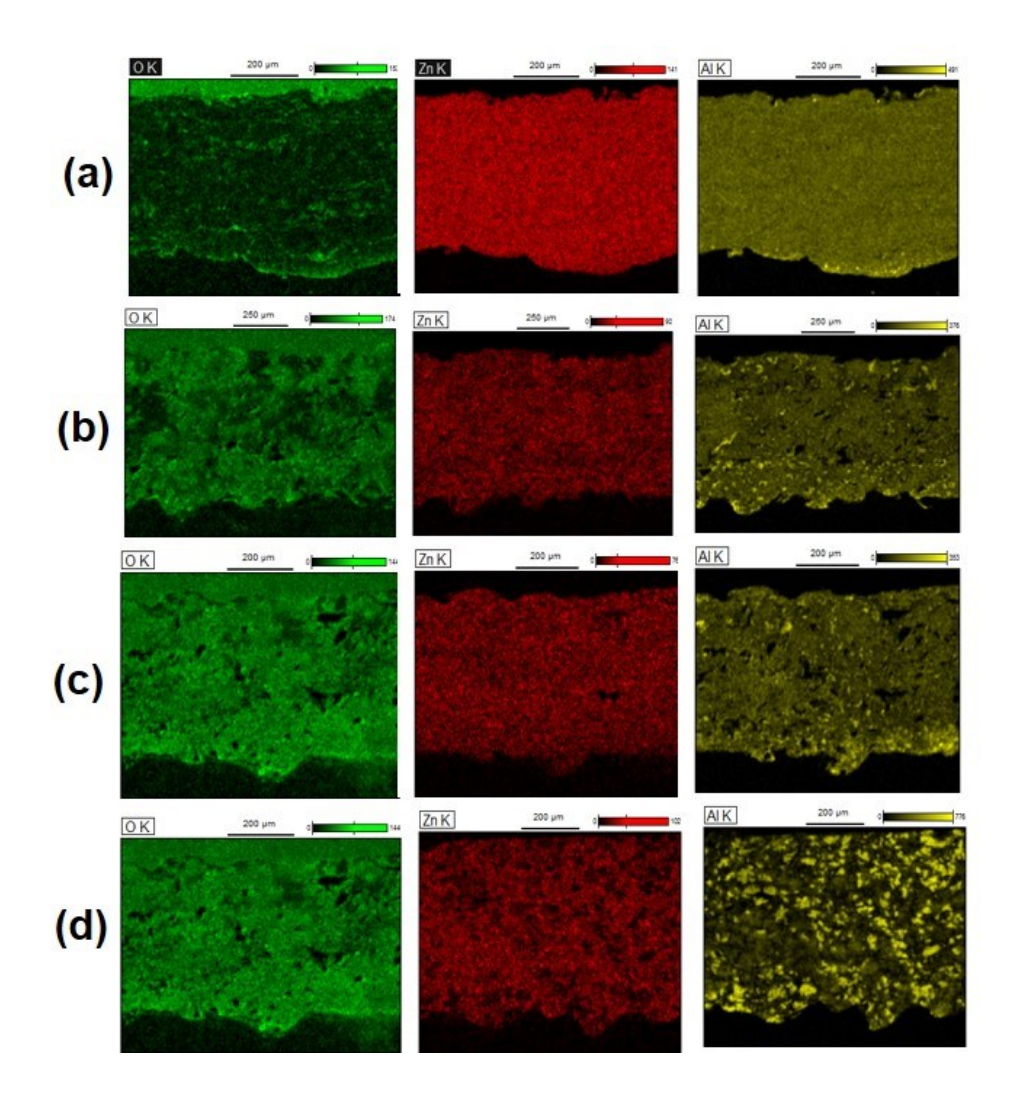


Fig. 8 Elemental distribution maps of oxygen, aluminum, and zinc on Zn-15Al coating cross-section for a) 25°C (in as-deposited condition) and after cooling from b) 300°C, c) 400°C, d) 500°C presenting the increase in oxidation and porosity in the coating microstructure with an increase in exposure temperature

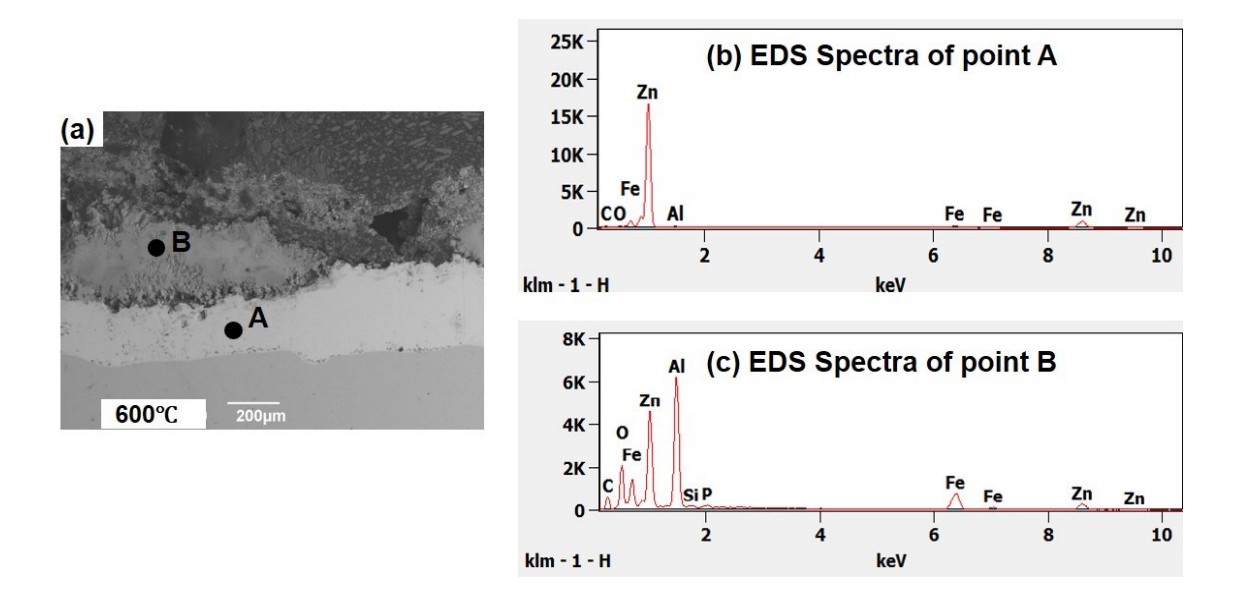


Fig. 9 a) SEM image of the Zn-15Al cross-section after cooling from 600°C, b) EDS spectra corresponding to point A on the coating cross-section, which shows that the light grey matrix is zinc-rich, and c) EDS spectra corresponding to point B on the coating cross-section, revealing that the corresponding coating matrix is highly oxidized and aluminum-rich

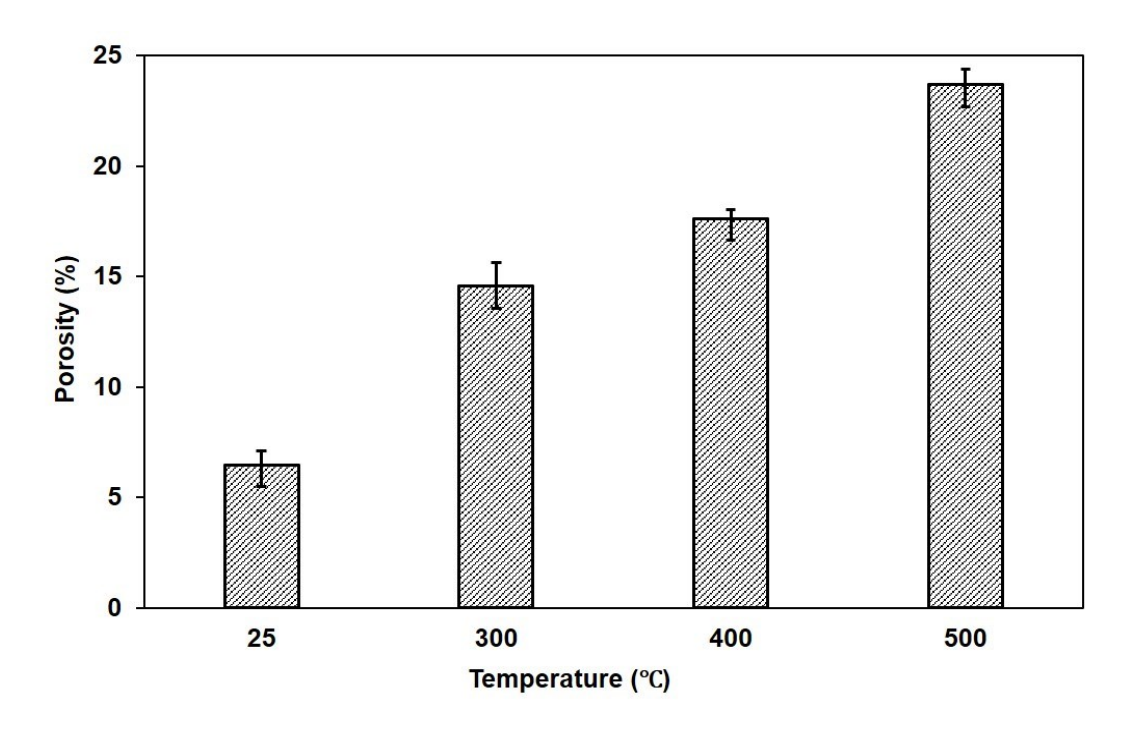


Fig. 10 Porosity changes in the Zn-15Al coating cross-section when subjected to different target elevated temperatures

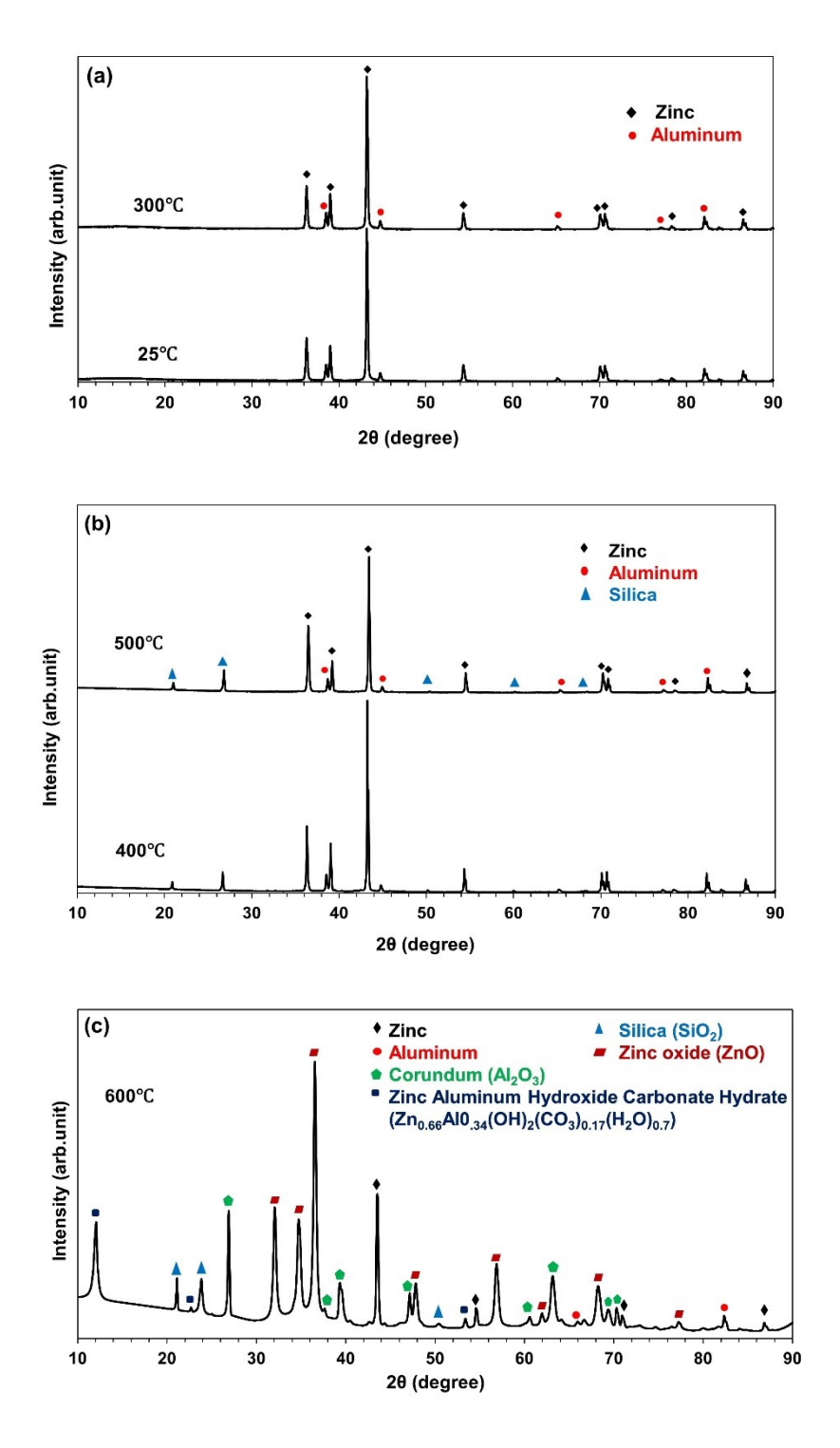


Fig. 11 XRD pattern from the surface of Zn-15Al coatings a) at 25°C (in as-deposited condition) and after cooling from 300°C, and b) 400°C and 500°C, and c) 600°C

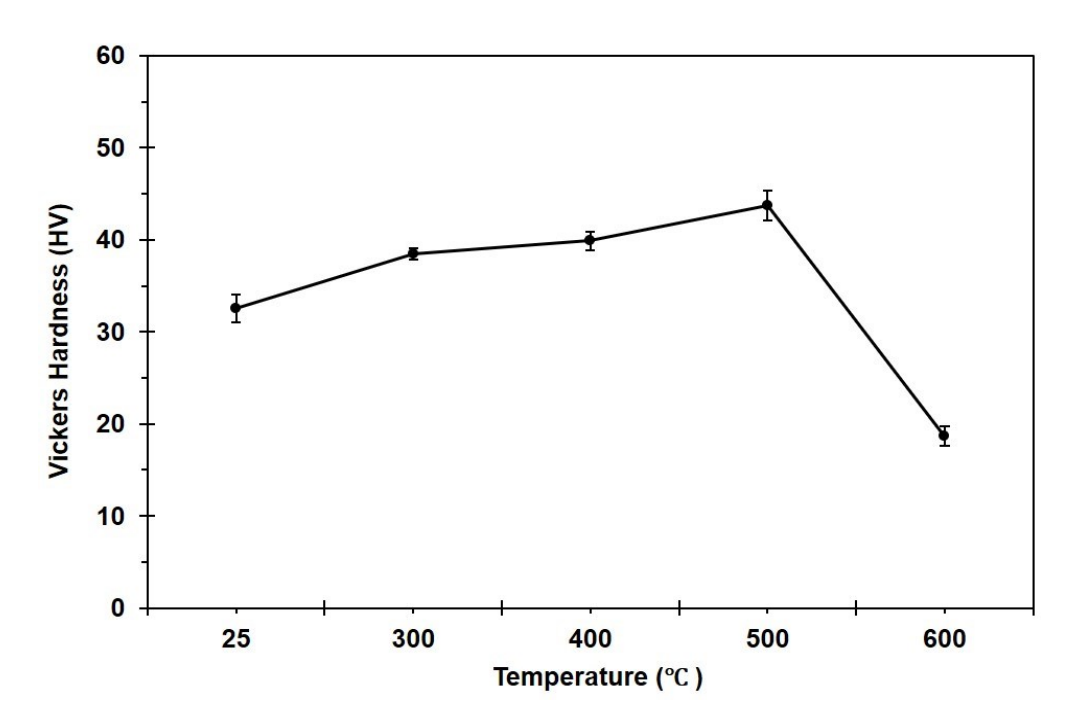


Fig. 12 Changes in Vickers hardness (HV) of Zn-15Al coatings with the increase in the exposed target elevated temperature

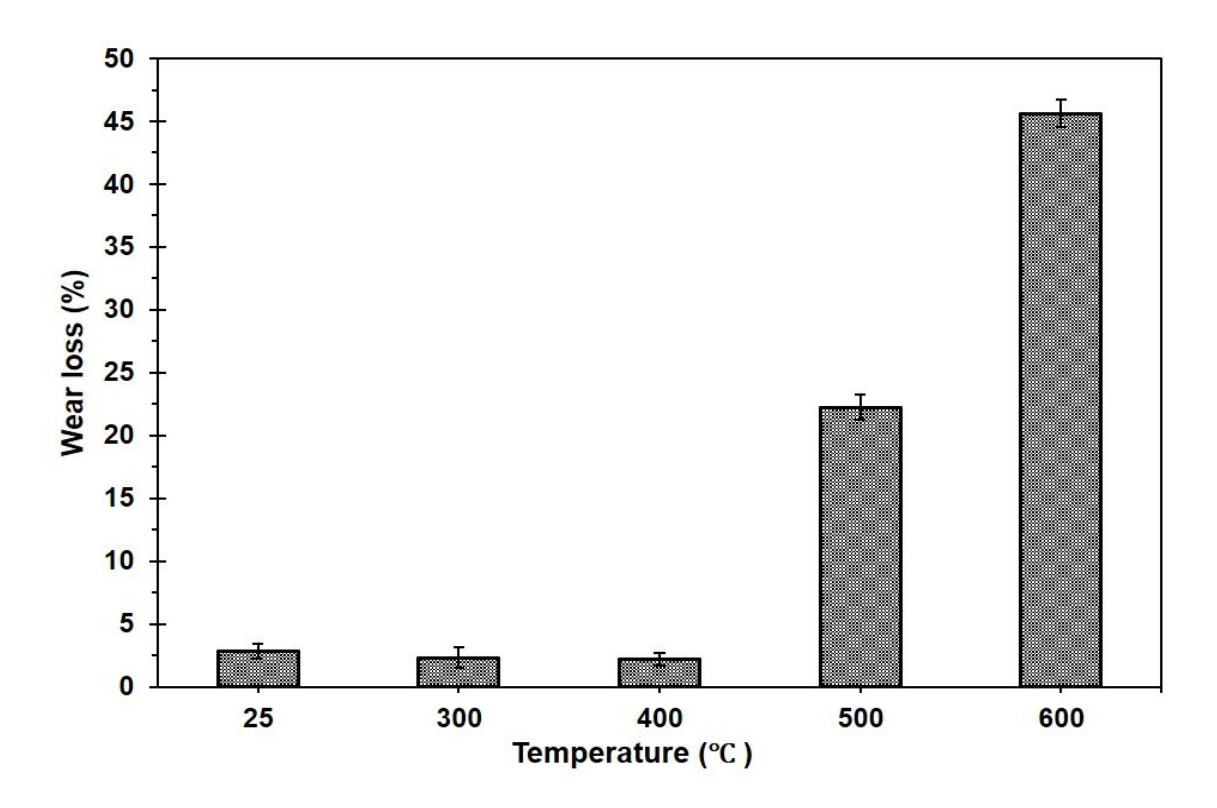


Fig. 13 Percentage of wear loss in Zn-15Al coatings exposed to different target elevated temperatures.

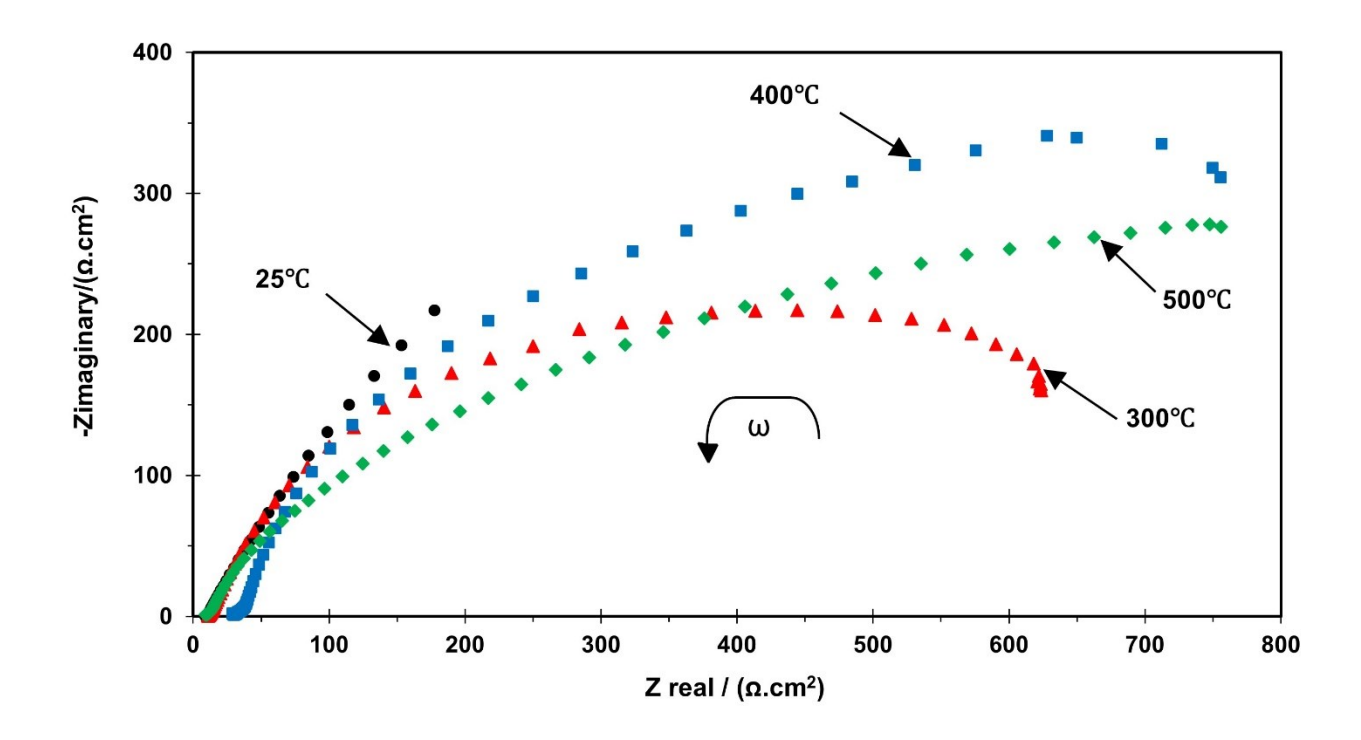


Fig. 14 Nyquist plot showing the changes in impedance values in Zn-15Al coating after exposure to different target elevated temperatures

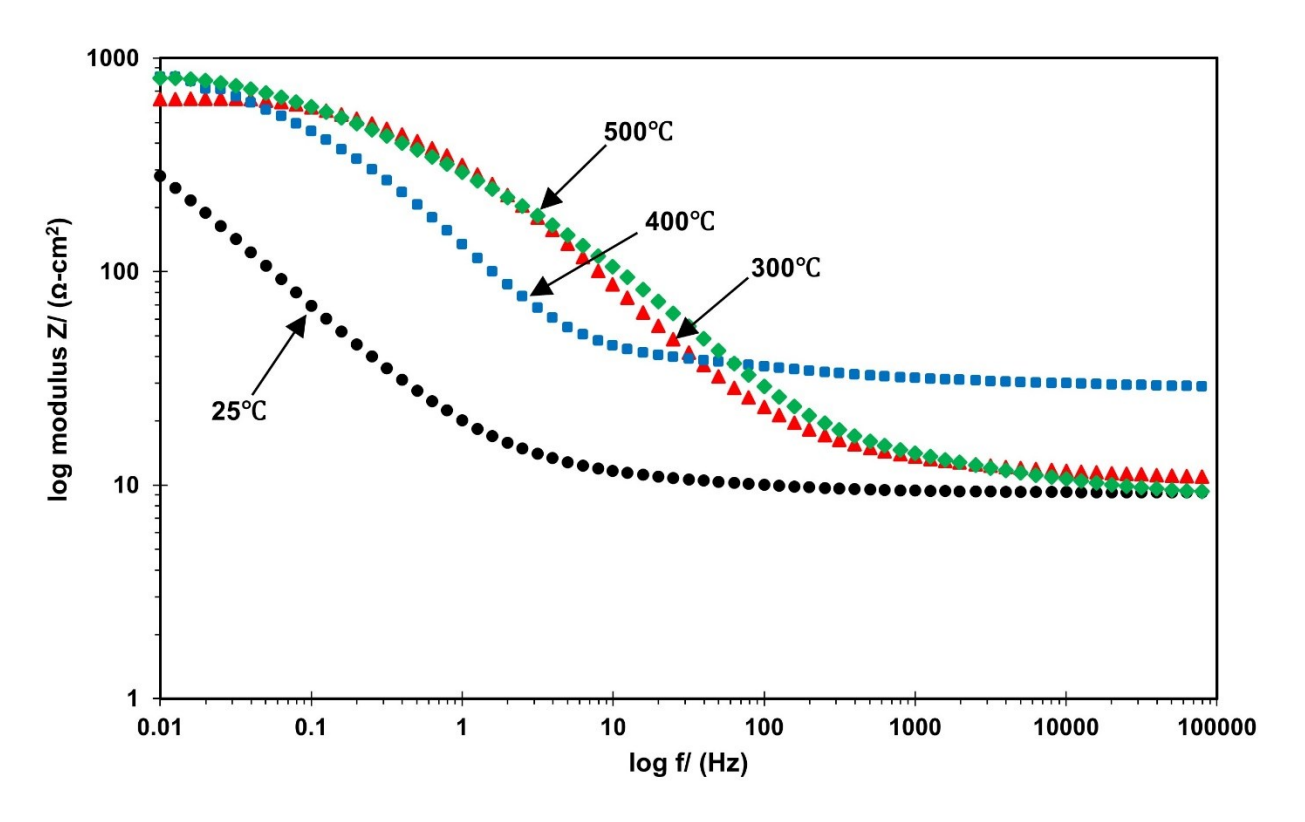


Fig. 15 Bode modulus plot of Zn-15Al coating after exposure to different target elevated temperatures

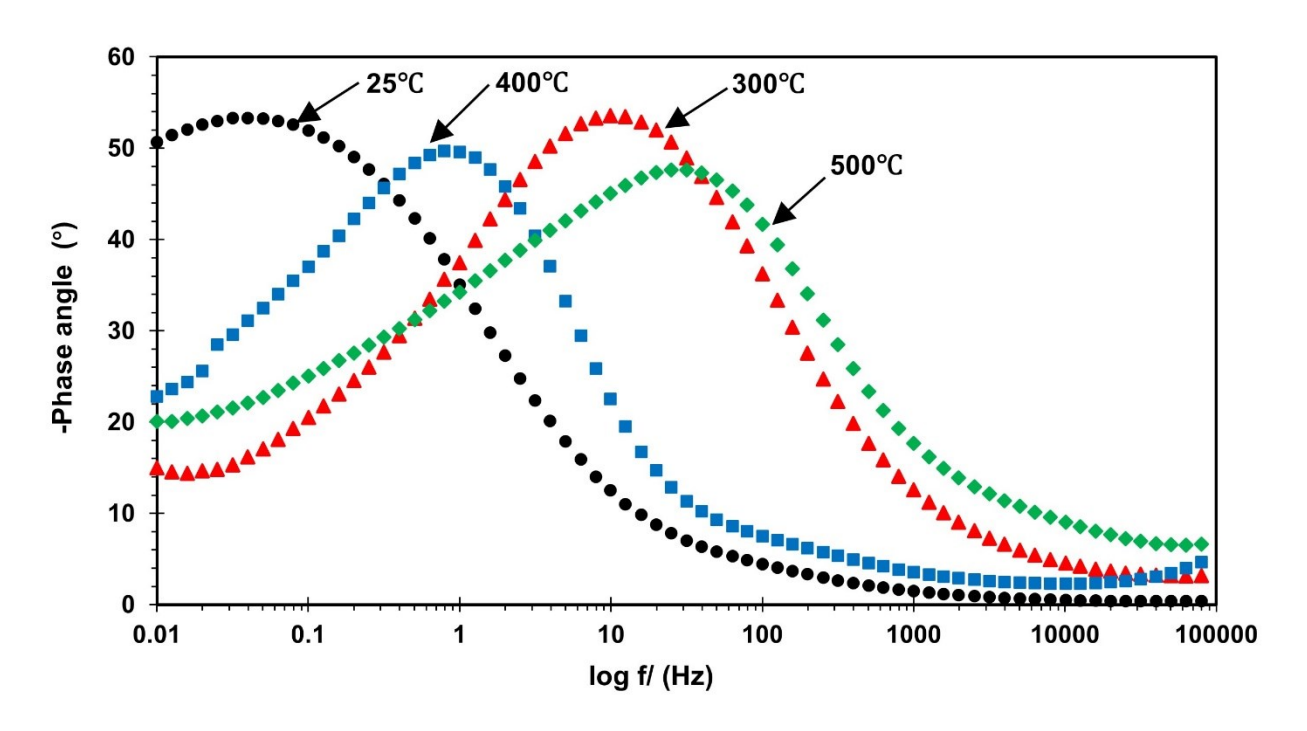


Fig. 16 Bode phase angle plot of Zn-15Al coating after exposure to different target elevated temperatures